Journal of Manufacturing Processes 14 (2012) 416–424

Contents lists available at SciVerse ScienceDirect

Journal of Manufacturing Processes

journal homepage: www.elsevier.com/locate/manpro

Technical paper

A prototype printer for laser driven micro-transfer printing

Reza Saeidpourazar[a], Michael D. Sangid[b], John A. Rogers[c], Placid M. Ferreira[d,*]

[a] Brooks Automation, Inc., Chelmsford, MA 01824, USA
[b] School of Aeronautics and Astronautics, Purdue University, West Lafayette, IN 47907-2045, USA
[c] Department of Materials Science and Engineering, Beckman Institute for Advanced Science and Technology, Frederick Seitz Materials Research Laboratory, University of Illinois at Urbana-Champaign, Urbana, IL 61801, USA
[d] Department of Mechanical Science and Engineering, University of Illinois at Urbana-Champaign, 1206 W. Green Street, MC-244, Urbana, IL 61801, USA

ARTICLE INFO

Article history:
Received 5 September 2012
Accepted 5 September 2012
Available online 12 October 2012

Keywords:
Micro-transfer printing
Thermo-mechanical delamination
Laser delamination
Flexible electronics
Component placement

ABSTRACT

This paper demonstrates a new mode of automated micro transfer printing called laser micro transfer printing (LμTP). As a process, micro-transfer printing provides a unique and critical manufacturing route to extracting active microstructures from growth substrates and deterministically assembling them into a variety of functional substrates ranging from polymers to glasses and ceramics and to metallic foils to support applications such as flexible, large-area electronics, concentrating photovoltaics and displays. Laser transfer printing extends micro-transfer printing technology by providing a non-contact approach that is insensitive to the preparation and properties of the receiving substrate. It does so by exploiting the difference in the thermo-mechanical responses of the microstructure and transfer printing stamp materials to drive the release of the microstructure or 'ink' from the stamp and its transfer to substrate. This paper describes the process and the physical phenomena that drive it. It focuses on the use of this knowledge to design and test a print head for the process. The print head is used to demonstrate the new printing capabilities that LμTP enables.

1. Introduction

In micro-transfer printing (μTP), a patterned viscoelastic stamp is used to pick up and transfer functional microstructures made by conventional microfabrication techniques in dense arrays on typical growth/handle substrates (such as silicon, germanium, sapphire or quartz) to a broad range of receiving substrates such as transparent, flexible and stretchable polymers, glass, ceramics and metallic foils. This provides an efficient pathway to the manufacture of flexible electronics and photovoltaics, transparent displays, wearable electronics, conformal bio-compatible sensors and many more [1,2]. Fig. 1 [1,2,5–8] provides a few examples of the types of devices or systems that are realized by transfer printing.

Fig. 2 shows a schematic of the process along with photographs of the donor substrate with microstructures (also referred to as 'ink') and a receiving substrate with printed microstructures. The transfer printing stamp is typically made of molded polydimethylsiloxane (PDMS) and patterned with posts to selectively engage microstructures on the donor substrate. The ink is picked up by adhesion to the PDMS posts. Printing occurs when the 'inked' stamp is subsequently brought into contact with a receiving substrate, followed by a slow withdrawal of the stamp. Adhesiveless transfer printing exploits the viscoelastic rate-dependent adhesion at the stamp–ink interface to enable either retrieval or printing via control of the separation velocity [3,4]. This approach to printing fabricated microstructures without adhesives simplifies downstream processing and is easily automatable by integrating on to a programmable, computer controlled positioning stage. Fig. 3 shows an automated micro-transfer printing machine developed at the University of Illinois. The major components of the system include (a) an automated *XY*-stage for positioning, (b) a *Z*-stage for moving the stamp up and down and controlling the separation speed and force, (c) an orientation stage that assists in obtaining parallel alignment between stamp and the receiving and donor substrates and (d) imaging system used for alignment and monitoring the printing process. The typical size of the printed inks ranges from 10s of microns up to the millimeter scale. The microstructure donor substrate is usually densely packed and can be of centimeter scale. The receiving substrate's dimensions are, in general, several times larger, especially when the ink is sparsely distributed on it. The stamp surfaces are typically patterned with posts with the same lateral dimensions as the microstructures being printed.

While the process is simple and easy to implement, its robustness is dependent on the properties and preparation of the surface of the receiving substrate. For successful printing, the adhesion between the ink and receiving surface must be sufficient to extract

* Corresponding author. Tel.: +1 217 333 0639.
E-mail addresses: saeidpour@gmail.com (R. Saeidpourazar), msangid@purdue.edu (M.D. Sangid), jrogers@illinois.edu (J.A. Rogers), pferreir@uiuc.edu (P.M. Ferreira).

1526-6125/$ – see front matter © 2012 The Society of Manufacturing Engineers. Published by Elsevier Ltd. All rights reserved.
http://dx.doi.org/10.1016/j.jmapro.2012.09.014

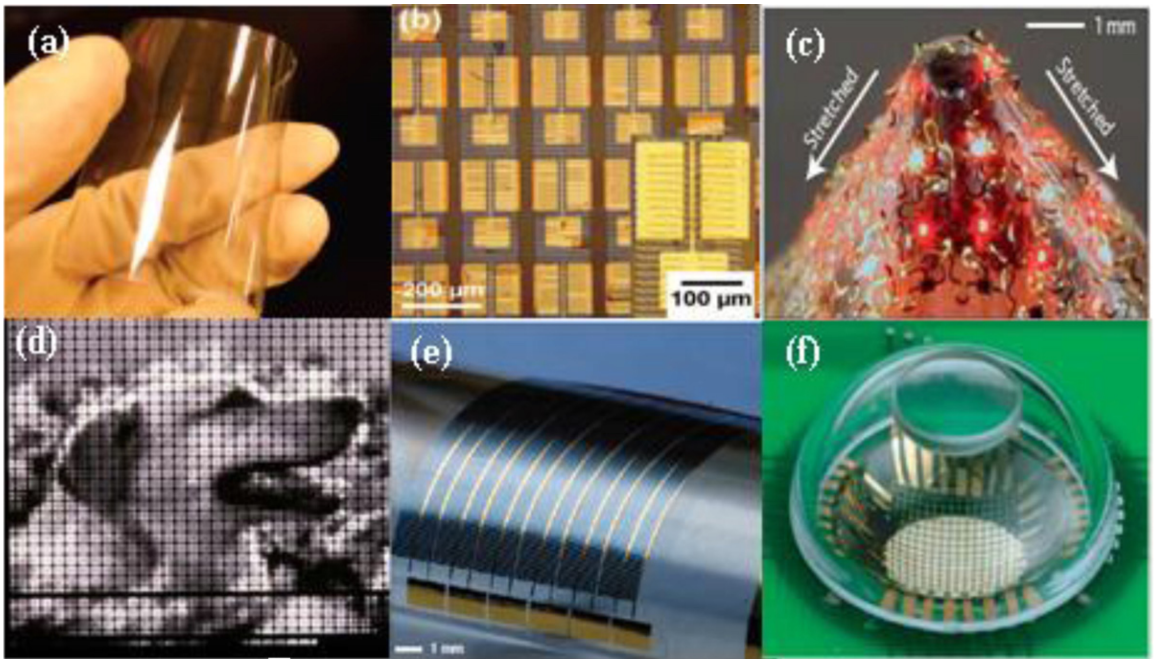

Fig. 1. Some examples of devices made using transfer printing. (a) Transparent carbon nanotube based transistors [5]. (b) GaN transistors on plastic substrate [7]. (c) LED on stretchable substrate [1]. (d) OLED display with printed electronics [6]. (e) Ultrathin silicon solar microcells [2]. (f) A hemispherical electronic eye camera [8].

the ink from the stamp and, when these conditions are satisfied, the surface much be clean and flat so that good contact is developed with the ink. Thus, printing on low-adhesion surfaces, patterned surfaces or soft gels can be challenging.

The process depicted in Fig. 2 can be scaled into a high transfer-rate, parallel printing process by increasing the number of posts on the stamp. As this parallelism increases, additional challenges accrue. Small misalignments between the substrate and the stamp get magnified as the size of the stamp increases causing substantial variations in the printing conditions at posts in different areas of the stamps leading to printing failures. Failure to print a microstructure in one cycle can result in repeated failures at that post in subsequent cycles, until the residual micro-structure is removed. When large receiving substrates are involved, waviness of the substrates gives rise to non-repeatable variability in printing conditions across the stamp. Finally, when large area expansions are involved, i.e., the printed microstructures has a high pitch or low areal density on the receiving substrates, the stamps used have posts that are spaced far apart and are therefore susceptible to stamp collapse [9,10], especially when larger printing forces are used to compensate for misalignments ('wedge' errors) between the stamp and the substrate. Such collapses result in the peeling out of microstructures by the stamp wherever contact occurs, and can damage both, the donor and receiver substrates.

In this paper, we develop a new, non-contact mode for this process that uses a laser to supply the energy required to drive the release of the ink from the stamp and its transfer to the receiving substrate. Since it does not rely on the strength of ink–substrate interface, created by mechanically pressing the ink onto the receiving substrate, to achieve its release from the stamp, the process does not depend on properties or the preparation of the receiving substrate for successful printing. Further, by using a scanned laser beam to address different inks or microstructures on the stamp, high-throughput modes of printing, not susceptible to small wedge errors between the stamp and the substrate, are possible. Thus, this new process mode that we call laser-driven micro-transfer printing (LμTP) has the potential to become a highly scalable, robust and versatile printing process.

The next section of this paper describes the laser transfer printing process and the phenomena it exploits. It also provides a detailed design of the laser print head for prototype laser transfer printing tool along with its calibration and testing. The third section demonstrates successful LμTP for situations that would be difficult to achieve with conventional transfer printing. It also explores one important parameter, separation of the stamp and receiving substrate on the accuracy of the transfer. Finally, conclusions and directions for future work are discussed.

2. Laser-driven micro-transfer printing

2.1. Process description

LμTP builds on micro-transfer printing technology [3,4]. It uses the same well-developed semiconductor processing technologies for creating donor substrates with dense arrays of printable microstructures, the same materials and techniques for fabricating the transfer stamps, and the stamps are 'inked' with microstructures using the same strategies [3,4]. The critical point of departure is the printing or transfer of the ink from the stamp to the receiving substrate. Instead of using mechanical means, LμTP uses a pulsed laser beam focused on the interface between the stamp and the microstructure to release and drive the microstructure to the receiving substrate. The wavelength of the laser is chosen so that the stamp material is transparent to the laser while the ink is absorbing. Here we choose an IR laser with wavelength 805 nm. Additionally, the stamp material is chosen so as to have a large mismatch in the coefficient of thermal expansion (CTE). For example, in the prototype reported here, single crystal silicon is used as the ink and PDMS as the stamp with CTEs of 2.6 ppm/°C and 310 ppm/°C respectively, to produce a CTE mismatch of two orders of magnitude.

Fig. 4 shows a schematic of the LμTP process. For printing step, the inked stamp is positioned so that the ink is close (about 6–10 μm) to the receiving substrate. A pulsed laser beam is then focused on the interface between the stamp and the ink to cause the transfer of the ink to the substrate. Since a PDMS stamp is

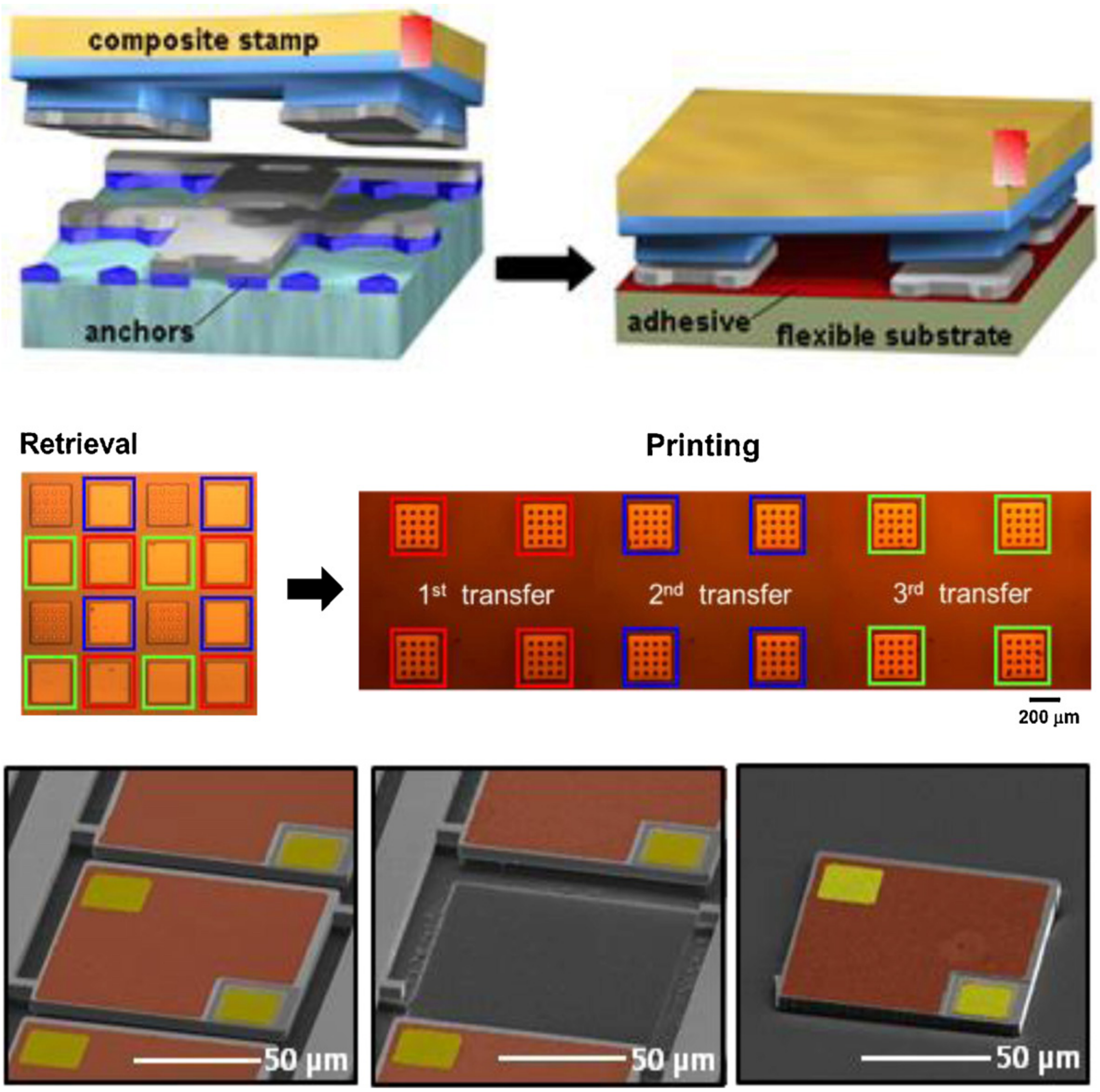

Fig. 2. (Top) A patterned stamp with 4 posts retrieves ink from a donor substrate and transfers it to a receiving substrate, (middle) results of 3 printing cycles displaying ink from a dense donor substrate, which is expanded on a receiving substrate, and (bottom) SEM images of representative micro-LED, shown in sequence, (left) donor substrate before retrieval, (center) after retrieval from the Si substrate, and (right) after transfer-printing onto a receiving substrate.

transparent in the near IR range, the laser radiation is transmitted through the stamp and is absorbed by the microstructure ink. As a result, the ink heats up and acts as a heat source for the PDMS stamp, conducting heat across the stamp–ink interface to raise the temperature of the PDMS stamp in the vicinity of the interface. The rise of temperature in the stamp and ink leads to thermal expansions in both. Due to the large CTE mismatch for the two materials ($\alpha_s = 310\,\mathrm{ppm}/^{\circ}\mathrm{C}$ [11] for PDMS and $\alpha_c = 2.6\,\mathrm{ppm}/^{\circ}\mathrm{C}$ for silicon [12]) and their free expansion being restricted by the contact interface between them, the thermal strain must be accommodated by bending (or the formation of a curvature) in the stamp–ink composite. This stresses the interface and, when the energy release rate due to delamination at the interface exceeds the work of adhesion of the interface, the ink is released from the stamp.

The use of laser driven delamination has been reported by other researchers. Bohandy [13] was the first to report such a laser-driven deposition process. Holmes and Saidam [14] reported a process called Laser-Driven Release and used it for printing prefabricated metal microstructures from a glass fabrication substrate on to a receiving substrate. Arnold and Piqué [15] have reported widely on what they call Laser-Induced Forward Transfer or LIFT process. In all these approaches, the driving mechanism is laser ablation at the interface. Much of the reported research uses pico- or femtosecond lasers and sacrificial layers at the microstructure–support structure (stamp) interface with a low vaporization temperature and a high absorptivity at the laser wavelength to enhance the delamination forces produced by ablation. The unique aspects, then, of LµTP, include:

it uses microsecond scale pulses and relies on a thermo-mechanical phenomenon based on thermal strain mismatch to drive the transfer printing process;

(a) being a lower temperature process (250–300 °C instead of temperatures reaching 1000 °C), less damage to active microstructures;
(b) the properties of the stamp are tuned to achieve both, extraction of ink from the donor substrate and deposition on to the receiving substrate;
(c) the stamp remains undamaged (because the process is driven by a reversible strain in the stamp rather than an irreversible

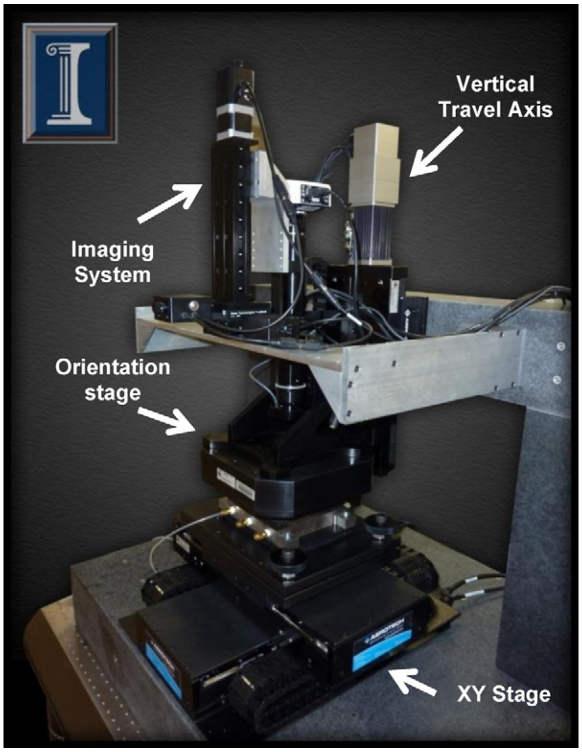

Fig. 3. Automated transfer printing machine showing the four axes of motion and integrated optics.

chemical change in it), thus enabling a repeated pick-and-place process mode.

Detailed modeling and analysis of the process are described in [23]. Here we concentrate on the design of the printing tool for the process.

2.2. Prototype laser micro-transfer printer design

A prototype LμTP was developed by designing a printhead and integrating it with a *XYZ* positioning stage. A schematic of the print head is shown in Fig. 5. The print head was developed so that printing could be observed through the stamp. The laser radiation is brought into the system via an optical cable from one side of the

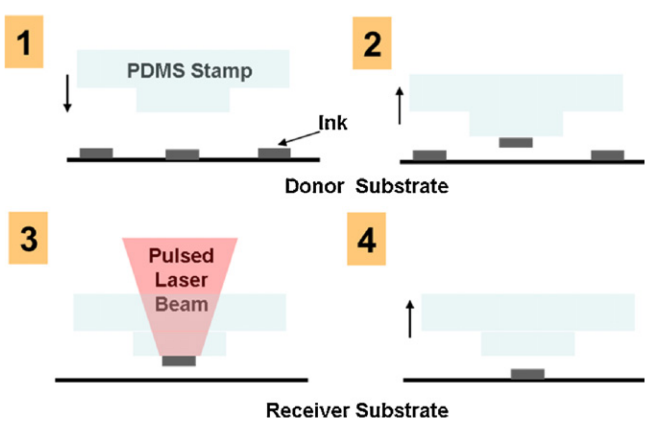

Fig. 4. Schematic of the LμTP steps: 1 – the PDMS stamp is aligned to the donor substrate and approaches it to pick up ink; 2 – ink is transferred to stamp; 3 – stamp is aligned to receiving substrate and laser pulse is used to heat up the ink–stamp interface; and 4 – ink is transferred to receiving substrate and stamp is withdrawn for next printing cycle.

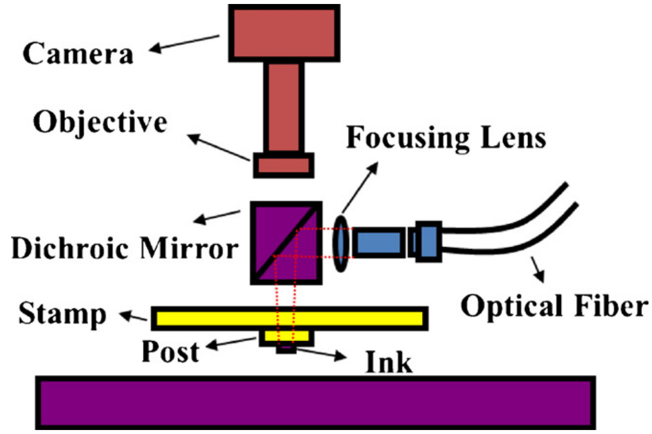

Fig. 5. A schematic of the print head for laser micro transfer printing. An optical cable is used to bring in the laser radiation from a laser diode in this proposed design.

print head. A dichroic mirror is used to direct the laser beam toward the stamp below it. A GRIN lens at the end of the optical cable is used to focus the laser beam on the ink.

One of the first steps in the realization of the schematic of the prototype print head of Fig. 5 is to estimate the power requirements (i.e., size the laser for the print head) and perform a first-cut analysis of whether or not a thermo-mechanical delamination process is possible without damaging the PDMS stamp. For this analysis (and for experimental verification) we use a single crystal silicon square with a lateral dimension of 100 μm and a thickness of 3 μm as our model/or representative ink. First, we compute the temperatures at which thermal mismatch strains in the Si–PDMS system give rise to energy release rates enough to overcome the work of adhesion at the Si–PDMS interface. We then compute the power of the laser system required to drive the steady state temperature of this system past the delamination temperature.

To compute the delamination temperature, we use the approach originally proposed by Stoney [16] for an infinitely thin film and modified by Freund [17] for finite film thickness. We use silicon as the thin film (thickness, $h_c = 3$ μm) and PDMS as the substrate (thickness, $h_s = 100$ μm) to model film delamination. As previously mentioned, the PDMS stamp has a higher coefficient of thermal expansion; thus, when heated, the PDMS would expand more than the Si ink, although the expansion is constrained due to a common interface shared by the two materials. As a result, strains accrue in both the materials. To estimate this strain, we assume a constant, uniform temperature distribution throughout the ink and the immediate vicinity of the post on the stamp. The strain energy exists solely because of an incompatible elastic mismatch strain that arises when the temperature is increased by an amount ΔT above room temperature (the conditions at which the interface was created) due to heating by laser pulse, as no external applied tractions or stresses exist in the system. Consequently, the Si chip undergoes a biaxial tensile stress; assuming the printing chip is an isotropic, elastic, homogenous material; its strain energy density at the interface is given by, $U(z = \frac{1}{2}h_s)$:

$$U\big|_{z=h_s/2} = \frac{E_c}{1-\upsilon_c}\left(\varepsilon_o - \kappa\frac{h_s}{2} + \varepsilon_m\right)^2 \qquad (1)$$

where the elastic modulus ($E_c = 179.4$ GPa) and Poisson ratio ($\upsilon_c = 0.28$) denote the elastic constants of silicon [3]. Hence, the strain energy density is composed of the mid-plane extensional strain, ε_o, the strain arising from the mismatch in thermal expansion coefficients between the chip and substrate, ε_m, and the curvature, κ, of the chip about a center of curvature equivalent to half of the substrate's thickness, $h_s/2$. The mismatch

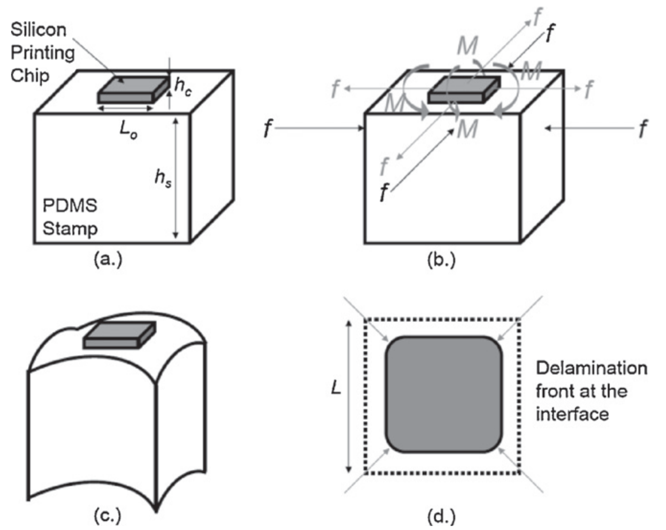

Fig. 6. Schematic of the thermal mismatch strains resulting in bending induced delamination of the silicon printing chip from the PDMS stamp. (a) Geometry of the initial setup. (b) Resulting forces and moments on the system as a result of the thermal mismatch strains. (c) To relieve strain energy, the system deforms in bending. The PDMS stamp is more compliant and as a result its curvature is more pronounced. (d) Deformation due to bending in the system produces delamination of the printing chip from the stamp. The delamination front at the interface moves from the corners of the chip toward its center.

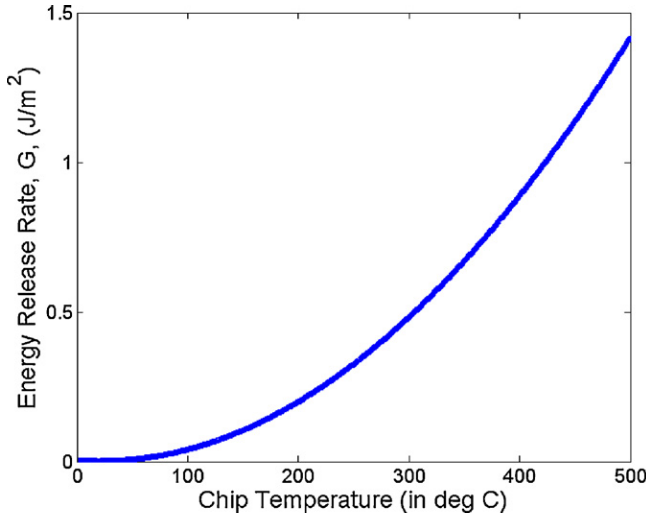

Fig. 7. The energy release rate of the PDMS-100 μm × 100 μm × 3 μm silicon ink–stamp system as a function of chip temperature is calculated by the finite-thickness correction to Stoney's formulation [16] by Freund [17].

in thermal expansion coefficients of the stamp and chip produces a strain, $\varepsilon_m = (\alpha_s - \alpha_c)\Delta T$.

The potential energy, V, is found by integrating Eq. (1) with respect to the height of the system. By taking the variants of the potential energy and checking for stability of the system (i.e. $\partial V/\partial\varepsilon_o = 0$ and $\partial V/\partial\kappa = 0$), we obtain two equations and two unknowns, the midplane extensional strain (ε_o) and the curvature (κ), that can be solved to yield.

$$\kappa = \frac{\kappa_{st}(1+h)}{1+4hm+6h^2m+4h^3m+h^4m^2}, \tag{2a}$$

$$\varepsilon_o = \frac{\varepsilon_{st}(1+h^3m)}{1+4hm+6h^2m+4h^3m+h^4m^2}, \tag{2b}$$

where $\kappa_{st} = (6\varepsilon_m/h_s)hm$ and $\varepsilon_{st} = -\varepsilon_m hm$

In these equations, shorthand notation is used where h ($=h_c/h_s$) and m ($= E_c^*(1-\upsilon_s)/E_s(1-\upsilon_c)$), refer to the ratios of the thicknesses and biaxial moduli of the chip to the substrate, respectively. Also, κ_{st} and ε_{st} refer to the solution of the Stoney equation, where the chip is infinitely thin. From this analysis, the stress in the chip at the interface is given by:

$$\sigma_c = \frac{E_c}{1-\upsilon_c}\left(\varepsilon_o - \kappa\frac{h_s}{2} + \varepsilon_m\right) \tag{3}$$

The strain energy accumulation in the system is relieved by deformation, giving rise to a curvature of the microstructure/stamp system, as shown in Fig. 6. The bending strain energy associated with this curvature produces the driving force for delamination at the ink–stamp interface. The energy release rate associated with such delamination due to relaxation of bending strain is given by:

$$G = \frac{1-\upsilon_c^2}{2E_c}(\sigma_c - \sigma_a)^2 h_c \tag{4}$$

where σ_a is the applied external stress, which is zero in this case. When this energy release rate is greater than the adhesion energy of the Si–PDMS interface, one can expect delamination to occur and the ink to be released from the stamp. We use the above analysis to arrive at a relationship between the energy release rate, G (J/m^2), and the temperature to which the system is raised above room temperature, ΔT (°C). This is shown in Fig. 7.

A number of investigators have reported values in the range of 0.05–0.4 J/m^2 for the adhesion energy of Si–PDMS interfaces [4,10,18–20]. From Fig. 7, if we choose a conservative value of 0.5 J/m^2 for G, we get a corresponding delamination temperature between 275 and 300 °C. This value is well within the range that PDMS can withstand without decomposing, especially for short, millisecond, durations [21].

In the description of the process, we stated that the laser heats up the Si ink that, in turn, heats up the interface and the PDMS in the vicinity. To do this, we used a COMSOL®[1] finite element model with the Si ink acting as the heat source. The strength of the heat source is varied and the corresponding steady state temperatures are computed. Fig. 8 shows the schematic of the model consisting of a 100 μm × 100 μm × 3 μm thick silicon chip is attached to a 200 μm × 200 μm × 100 μm high PDMS post. The bottom surface of the PDMS stamp (in Fig. 8) is fixed and the bottom surface of the silicon ink is constrained to move with the top surface of the post on the PDMS stamp. Other surfaces in this model are free to move. The heat source in the model is the square-shaped area at the stamp–ink interface. The exposed surfaces of the silicon and PDMS lose heat to the surroundings by convection. The model uses 75,000 nodes to perform a transient heat transfer analysis in COMSOL 3.5 for run intervals up to 5 ms (our typical laser pulse times range from 1 to 5 ms) with the silicon ink, PDMS and surroundings initially at 27 °C. Fig. 8 shows the results of one run, in which 135 mJ of heat is input into the system over a 3.4 ms interval. From this simulation, one can see that the temperatures reached in the system are about 584 °K, slightly higher than 300 °C, sufficient to cause delamination without damaging the stamp.

From this value of heat input rate, that we approximate to 150 mJ over 4 ms or 0.0375 W we can now calculate the power required in the laser pulse. To do so, we need to account for reflective and transmission losses as well as for the intensity distribution in the beam. For 800 nm radiation, the coefficient of absorption for silicon, $\alpha_c = 10^3$ cm^{-1} or its absorption depth is about 10 μm. The intensity

[1] Registered Trademark of The COMSOL Group.

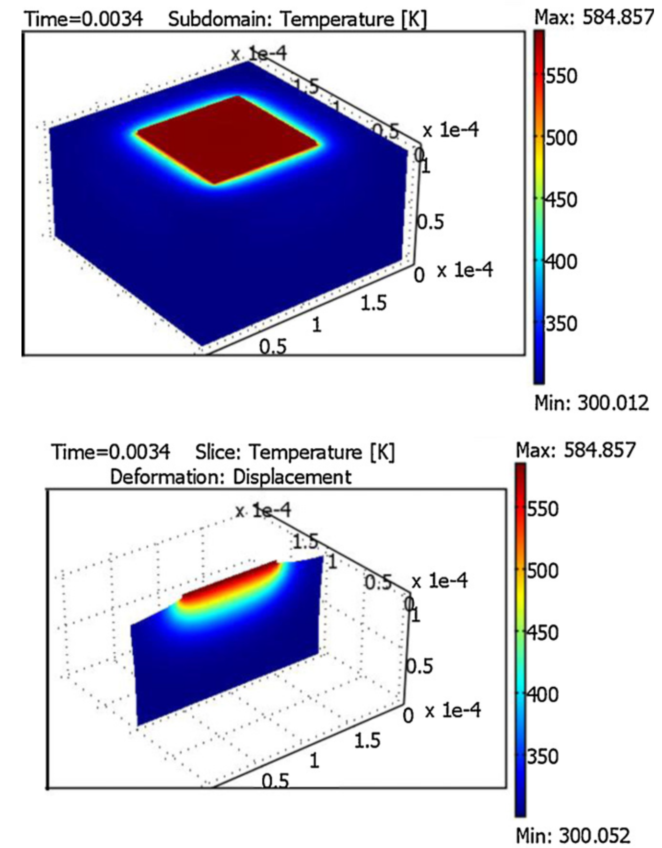

Fig. 8. Finite element model of the post and ink showing (top) temperature gradient in the post and attached ink and, (bottom) a slice of the post showing the temperature gradients and the deformed.

of the radiation emerging from a 3 μm thick sheet of silicon as a fraction of the intensity of the incident radiation, I_0, is given by:

$$\frac{I}{I_0} = \exp(-\alpha_c h) \tag{5}$$

which for $h = 3$ μm becomes approximately 0.75. With 75% of the radiation lost to transmission, only 25% of the radiation that enters the silicon is available for heating the ink. Next we deal with the fraction of the beam area that is incident on the silicon ink. The major consideration here is to uniformly heat the ink across its lateral dimension. If one considers a Gaussian beam, then too small of a beam diameter will result in a hot spot at the center of the ink. The power, $P(r)$, contained within a radius r of the beam is given by (see, for example, [22]):

$$P(r) = P(\infty)\left[1 - \exp\left(\frac{-2r^2}{\omega_0^2}\right)\right] \tag{6}$$

where $P(\infty)$ is the total power in the beam and ω_0 is the beam radius. For $r = 0.23\omega_0$, the intensity drop from the beam center to the perimeter of the circle is 0.1 or 10%. This will provide relatively uniform heating, but only 10% of the beam energy is contained in the circle. Finally, one must deal with the reflectivity of polished silicon, which at 800 nm is 0.328. Thus only 67.2% of the radiation incident on the ink is absorbed by, or transmitted through, it.

In summary, to provide the required 0.0375 W of heating, the beam power in the plane of the ink–stamp interface must be:

$$P = \frac{0.0375}{0.25 \times 0.1 \times 0.672} \simeq 2.25\,\mathrm{W} \tag{7}$$

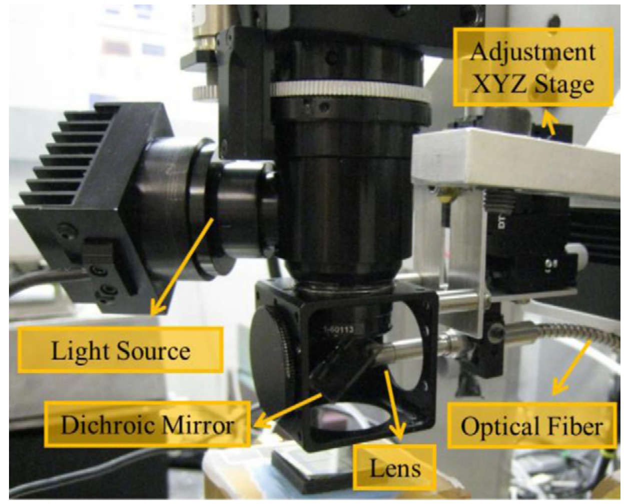

Fig. 9. Photograph of the laser micro-transfer print head.

Thus, it is not only feasible to perform thermo-mechanically delaminate the model silicon ink from the PDMS stamp by exploiting the mismatch in CTEs, it is possible to do so with a moderately powered diode laser.

Fig. 9 shows a photograph of the print head. A Jenoptik® continuous wave, fiber-coupled (fiber core diameter of 0.2 mm), passively cooled, 808 nm 30 W laser diode with electronic pulse control is used. A higher power rating was chosen to be able to account for losses in the coupling and cable, accommodate different materials and thinner and larger lateral dimension inks. The pulse resolution for the laser is 1 ms. The print head is integrated on to a custom-assembled, gantry-type *XYZ* positioning stage. The stage has 1 μm resolution, 150 mm of travel in the *X* and *Y* direction and 100 mm of travel in the *Z* direction. It is fitted with high (1 mm) resolution optics, capable of observing the process through the stamp. Except for the difference in the print head, the structure of the printer is very much like that shown in Fig. 3.

2.3. Calibration and testing

The prototype printer along with the laser printing head is calibrated to relate the beam power available at the ink–stamp interface for different current settings of the laser. Also, the validity numbers used in the analysis and design of the printer are verified.

To relate the current settings on the laser and the beam energy as it arrives at the stamp–ink interface, a photodiode power meter with a pre-calibrated reader (Thorlabs PM100D) is used, as shown in the schematic of Fig. 10. This power meter is chosen to have a very fast response time (<200 ns) compared to the laser pulse width (typically >1 ms), high optical power range (5 μW to 5 W) to withstand the intensity of the beam, high resolution (1 nW) and large inlet aperture (Ø12 mm) to be able to easily capture the entire laser beam during a pulse. A data acquisition card captures the analog output of the calibrated reader at a sampling rate of 40 kHz and stores it on a PC for subsequent analysis. The laser pulse time is set to 10 ms and the laser is pulsed with different current settings. The readings taken are averaged after those corresponding to the first and last milliseconds of the pulse are deleted to get rid of transients. This is repeated three times for each current setting. As can be seen in Fig. 10, the relationship between beam-power at the ink–stamp interface and the current setting for the laser is linear, with a threshold current of 5 amps. The calibration is done in the current range of 5 amps to 13 amps, with the beam power ranging from 0 to 5.25 W (sufficient for laser printing, with our model inks).

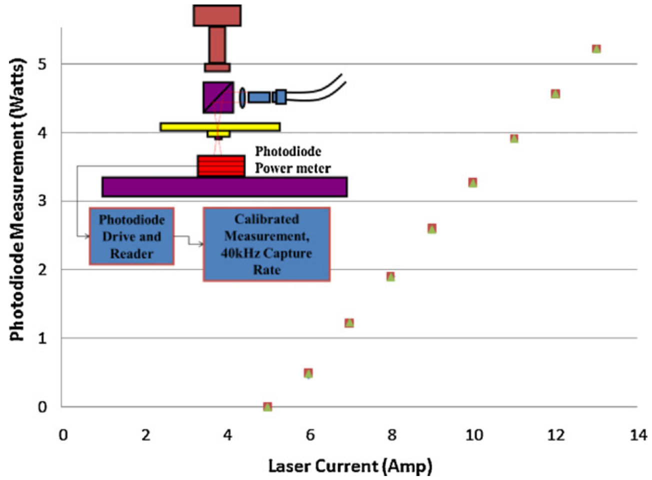

Fig. 10. Beam power at the stamp–ink interface plane as a function of the laser current.

To verify the delamination conditions previously stated, a two-step experiment is performed. The model ink ($100\,\mu m \times 100\,\mu m \times 3\,\mu m$ silicon square) is loaded on to the stamp using the standard transfer printing pick-up step [3,4]. Next the printing step is attempted. Here the pulse duration is set to 4 ms and pulses of increasing power (obtained by gradually increasing the current) are used until the power level at which transfer occurs is reached. This gives us the minimum energy input settings for a 4 ms pulse at which transfer of the ink takes place. After this, the receiving substrate is replaced with the photodiode power meter and two laser power recordings are made with the same pulse times but a current setting just a little bit lower than that needed to achieve transfer. The first measurement is made with the beam passing through an empty stamp and the second is made with the ink on the stamp. Integrating the power measures across the duration of the pulse gives us the total energy arriving at the power meter due to the pulse. The difference between the total energy arriving at the photometer with and without the ink gives us the sum of the energy reflected and absorbed by the ink. Knowing the reflectivity, we can obtain the energy absorbed by the ink and available for heating the ink. Also, in Eq. (7) we had computed the beam power at the plane of the ink–stamp interface required for delamination and transfer to be around 2.25 W. Examining the power recording will allows us to verify the design.

Fig. 11 shows the power recordings by the photodiode power meter. Integrating the areas under the curves, it can be seen that the difference in energy reaching the power meter is 0.224 mJ. Accounting for the reflectance of the silicon inks, we get 0.134 mJ of energy available for heating the ink, a value very close to that predicted by the thermo-mechanical delamination analysis. Additionally, from this recording, it can be see that the beam power required for delamination is around 2.5 W, while 2.25 W was the computed power requirements. Thus, the approach to designing the print head can be considered to be reasonably accurate.

3. Demonstrating LμTP

LμTP provides new capabilities for transfer printing technology. As previously claimed, it is relatively independent of the properties and topography of the receiving surface. Hence, it should be possible to print on surfaces with low adhesion energy, structured surfaces where contact area is a small fraction of the surface, non-flat surfaces. Each of these cases was tested and demonstrated to be feasible. Additionally, the possibility of printing on liquids and gels is also demonstrated. Finally, positional errors for printing on low adhesion energy are experimentally characterized. We used the model ink, $100\,\mu m \times 100\,\mu m \times 3\,\mu m$ Si squares, for these demonstrations. Further, the printing for these demonstrations was conducted with the pulse times set to 4 ms, and the power level set to 2.5 W.

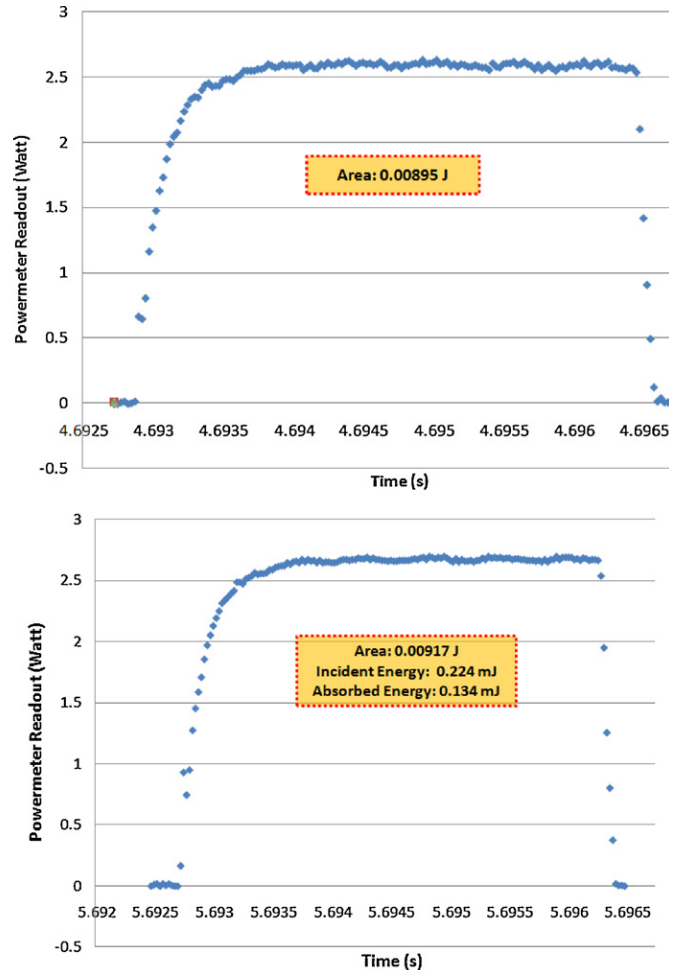

Fig. 11. Power recordings for 4 ms laser pulses with current setting at 10 amps with ink on stamp (top) and with a bare stamp (bottom). The difference in areas under the power curves gives the energy absorbed and reflected by the ink.

Printing silicon inks on silicon surfaces is generally difficult with flat PDMS stamps because of the low adhesion at the Si–Si interfaces. It is easily accomplished by the LμPT process. Fig. 12(a) shows a small array of silicon chips printed on to a silicon substrate to bridge gold traces that were pre-patterned on the surface. Fig. 12(b) shows a multi layered structure of silicon squares which would be extremely challenging to achieve with conventional transfer printing as contact is made only at the corners of the squires. Fig. 12(c) demonstrates the printing of a silicon chip between two pedestals.

To demonstrate printing of inks on non-flat surfaces printing on spherical surfaces, including the surface of a liquid droplet was performed. Fig. 13 shows some results where silicon squares are successfully printed on individual spheres, a non-uniform array of beads and on the surface of a NOA droplet.

Finally, to demonstrate printing on partial and recessed surfaces, a number of substrates with different features were prepared. Fig. 14 shows examples of printing on ledges, beams and inside concave features. Some of these printing demonstrations exhibit the kind of precise placement that the process is capable of producing. This precision in placement is dependent on a number of

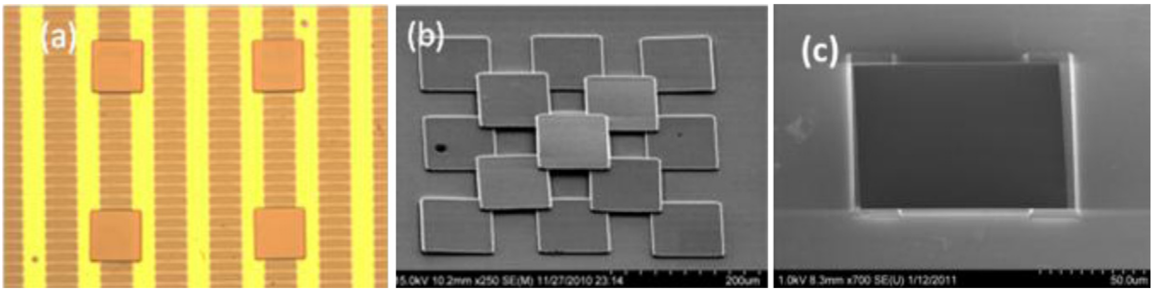

Fig. 12. Examples of structures constructed by laser micro-transfer printing. (a) Optical micrograph of silicon squres printed on a silicon substrate with gold traces; (b) a 3-D pyramidal structure built of silicon squires; and (c) a bridge structure build by printing a silicon plate on two bars patterned on a silicon substrate. (*Scale*: silicon squares in micrographs have sides of 100 μm.)

Fig. 13. Examples of printing on curved surfaces, (left) printing on a single 1 mm ceramic sphere, (middle) printing on a non-uniform array of 500 μm silica beads, and (right) printing on to a liquid NOA droplet. (*Scale*: in all the micrographs, the printed squares have sides of 100 μm.)

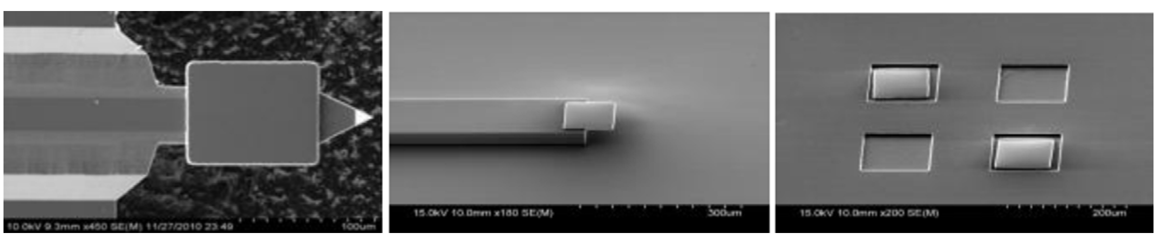

Fig. 14. Examples of printing on partial and recessed surfaces. (Left) A silicon square printed on to a AFM cantilever, demonstrating assembly on an active structure, (middle) printing on a ledge, and (right) printing into recessed spaces. (*Scale*: in all the micrographs, the printed squares have sides of 100 μm.)

set-up factors such as precise centering of the beam on the ink. It is also dependent on process variables, the key variable being the 'stand-off' or distance of the stamp from the receiving substrate. To characterize this dependence, printing was performed at the lowest energy for reliable delamination (4 ms pulses with the power setting at 2.5 W and the same model ink) with different stand-off heights on to a substrate patterned with fiducials. First the stamp is brought into close to the substrate and aligned to the fiducial on the substrate using the optics on the printer (about 1 μm resolution) and the positioning stages (also 1 μm resolution). It is then withdrawn to the appropriate height and transfer printed. The error in the transfer process is obtained through image analysis of frames taken after alignment (with the ink still on the stamp) and after printing. This experiment is conducted for different stand-off heights ranging from 5 μm to 300 μm, with 5 repetitions at each stand-off height. Fig. 15 shows the observed dependence of transfer errors on printing stand-off height. Within the resolution of experimental observations, the transfer errors become insignificant at stand-off heights of about 20 μm.

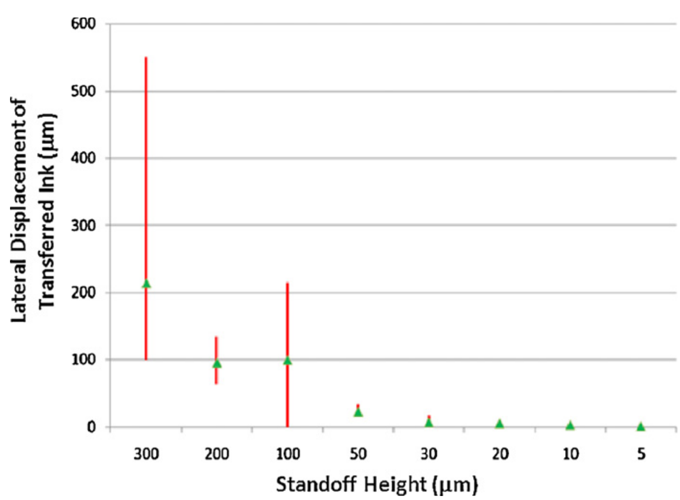

Fig. 15. Lateral transfer errors as a function of stand-off height.

4. Conclusions

In this paper we have demonstrated a new mode of transfer printing and prototyped an automated transfer printing machine to implement it. In this mode of micro-transfer printing, a laser supplies the energy to drive a thermo-mechanical delamination process that releases the ink from the stamp and transfers it to the receiving substrate. A procedure for designing the print head is developed and verified. This new printing mode that we call laser micro-transfer printing (LμTP) extends the versatility of micro transfer printing by making the process virtually independent of the properties and preparation of the receiving substrate. Thus, printing on low adhesion surfaces, curved, partial and recessed surfaces, operations that are typically difficult in more conventional modes of the process, are easily performed in this process mode as demonstrated on a prototype laser micro-transfer printer. With successful demonstration of this process, process studies are underway to understand and parameterize the process.

References

[1] Kim R-H, Kim D-H, Xiao J, Kim BH, Park S-I, Panilaitis B, et al. Waterproof AlInGaP optoelectronics on stretchable substrates with applications in biomedicine and robotics. Nature Materials 2010;9:929–37.

[2] Yoon J, Baca AJ, Park S-I, Elvikis P, Geddes JB, Li L, et al. Ultrathin silicon solar microcells for semitransparent, mechanically flexible and microconcentrator module designs. Nature Materials 2008;7:907–15.

[3] Meitl MA, Zhu ZT, Kumar V, Lee KJ, Feng X, Huang YY, et al. Transfer printing by kinetic control of adhesion to an elastomer stamp. Nature Materials 2006;5:33–8.

[4] Kim S, Wu J, Carlson A, Jin SH, Kovalsky A, Glass P, et al. Microstructured elastomeric surfaces with reversible adhesion and examples of their use in deterministic assembly by transfer printing. Proceedings of the National Academy of Sciences of the United States of America 2010;107(40):17095–100.

[5] Ishikawa FN, Chang HK, Ryu K, Chen PC, Badmaev A, De Arco LG, et al. Transparent electronics based on transfer printed aligned carbon nanotubes on rigid and flexible substrates. ACS Nano 2009;3:73–9.

[6] Bower CA, Menard E, Bonafede E. Active-matrix OLED display backplanes using transfer-printed microscale integrated circuits. In: Proceeding of the 59th Electronic Component and Technology Conference. 2010.

[7] Lee KJ, Meitl MA, Ahn JH, Rogers JA, Nuzzo RG, Kumar V, et al. Bendable GaN high electron mobility transistors on plastic substrates. Journal of Applied Physics 2006;100(12), 124507–124507-4.

[8] Ko HC, Stoykovich MP, Song J, Malyarchuk V, Choi WM, Yu C-J, et al. A hemispherical electronic eye camera based on compressible silicon optoelectronics. Nature 2008;454:748–53.

[9] Hsia KJ, Huang Y, Menard E, Park J-U, Zhou W, Rogers J, et al. Collapse of stamps for soft lithography due to interfacial adhesion. Applied Physics Letters 2005;86(15):1900303.

[10] Huang Y, Zhou W, Hsia KJ, Menard E, Park J-U, Rogers J, et al. Stamp collapse in soft lithography. Langmuir 2005;21(17):8058–68.

[11] Mark JE, editor. Polymer data handbook. New York: Oxford University Press; 1984.

[12] Okada Y, Tokumaru Y. Precise determination of lattice parameter and thermal expansion coefficient of silicon between 300 and 1500 K. Journal of Applied Physics 1984;56(2):314–20.

[13] Bohandy J, Kim BF, Adrian FJ. Metal deposition from a supported metal film using an excimer laser. Journal of Applied Physics 1986;60: 1538.

[14] Holmes AS, Saidam SM. Sacrificial layer process with laser-driven release for batch assembly operations. Journal of Microelectromechanical Systems 1998;7(4):416–22.

[15] Wartena R, Curtright AE, Arnold CB, Piqué A, Swider-Lyons KE. Li-ion microbatteries generated by a laser direct-write method. Journal of Power Sources 2004;126(1–2):193–202.

[16] Stoney GG. The tension of metallic films deposited by electrolysis. Proceedings of the Royal Society of London Series A 1909;82(553): 172–5.

[17] Freund LB, Suresh S. Thin film materials – stress, defect formation, and surface evolution. Cambridge: Cambridge University Press; 2003.

[18] Chaudhury MK, Whitesides GM. Direct measurement of interfacial interactions between semispherical lenses and flat sheets of poly(dimethylsiloxane) and their chemical derivatives. Langmuir 1991;7(5):1013–25.

[19] Armani D, Liu C, Aluru N. Re-configurable fluid circuits by PDMS elastomer micromachining. In: MEMS'99 twelfth IEEE international conference. 1999. p. 222–7.

[20] Deruelle M, Leger L, Tirrell M. Adhesion at the solid–elastomer interface: influence of the interfacial chains. Macromolecules 1995;28: 7419–28.

[21] Camino G, Lomakin SM, Lazzari M. Polydimethylsiloxane thermal degradation. Part 1. Kinetic aspects. Polymer 2001;42:2395–402.

[22] http://www.rpgroups.caltech.edu/courses/aph162/2007/Protocols/Optics/e3872_Gaussian-Beam-Optics.pdf.

[23] Saeidpourazar R, Li R, Li Y, Sangid MD, Lu C, Huang Y, et al. Laser-driven noncontact transfer printing of prefabricated microstructures. IEEE/ASME Journal of Microelectromechanical Systems 2012;21(4):1049–58.